Liu *et al. BMC Genomics* (2025) 26:352
https://doi.org/10.1186/s12864-025-11546-5

BMC Genomics

RESEARCH Open Access

Identification of the ADH gene family in *Trichosporon asahii* and the role of *TaADH_like* in pathogenicity and fluconazole resistance

Zhen Liu[1†], Xiaoping Ma[1*†], Xiangwen Zeng[1†], Zhiguo Li[1], Ruiguo Liu[1], Rongyan Luo[1], Weichen Wang[1], Muhammad Salman Tahir[1], Chengdong Wang[2] and Yu Gu[3*]

Abstract
Alcohol dehydrogenase has been studied in regulation of fungal growth and development, stress response and pathogenesis, but its function in *T. asahii* remains unexplored. In this study, we analyzed the ADH gene family in *T. asahii* for the first time, identifying six *ADH* genes and containing conserved ADH_N and ADH_Zinc_N domains. We constructed an overexpression strain of the most significantly differentially expressed gene *TaADH_like* and compared its phenotypes with those of the wild-type strain, focusing on colony morphology, biofilm biomass, stress response, drug resistance, and pathogenicity. The results showed that *TaADH_like* overexpression reduced sensitivity to hypoxic conditions, altered the hyphae-to-yeast transition, and led to slower growth, decreased colonization ability, reduced tissue damage, and lower lethality. Increased osmotic stress sensitivity and the involvement of the HOG MAPK pathway in the hyphae-to-yeast conversion contributed to the reduced colonization capacity of *T. asahii*. Furthermore, the overexpression of *TaADH_like* promoted biofilm formation and led to a slight enhancement in fluconazole resistance in *T. asahii*. This study is the first to elucidate the function of the alcohol dehydrogenase gene in *T. asahii*, providing a foundation for future genetic research on this pathogen.

Keywords *Trichosporon asahii*, Alcohol dehydrogenase, ADH gene family, Hyphae-to-yeast conversion, Gene function

[†]Zhen Liu, Xiaoping Ma and Xiangwen Zeng contributed equally to this work.

*Correspondence:
Xiaoping Ma
mxp886@sicau.edu.cn
Yu Gu
guyu632@sicau.edu.cn
[1]Key Laboratory of Animal Disease and Human Health of Sichuan Province, College of Veterinary Medicine, Sichuan Agricultural University, Chengdu 611130, China
[2]China Conservation and Research Center for the Giant Panda, Chengdu 611800, China
[3]College of Life Sciences, Sichuan Agricultural University, Chengdu 611130, China

Introduction

Trichosporon asahii (*T. asahii*) belongs to the genus Trichosporon, which is widely found in nature and can colonize both animals and humans, invading the host through medical and surgical infections to cause disease [1]. It causes disseminated trichosporonosis, a complex fungal infection that can involve multiple organs, including superficial skin and hair infections, osteomyelitis, keratitis, meningitis, and endocarditis [2–5]. In recent years, an increasing number of clinical isolates have shown insensitivity to fluconazole in vitro drug sensitivity tests, leading to treatment failure in patients with invasive *T. asahii* infections [6, 7].

Alcohol dehydrogenase (ADH, EC 1.1.1.1), a zinc-containing enzyme that catalyzes the interconversion of aldehydes and alcohols, is ubiquitous in fungi, plants, and mammals. It plays critical roles in growth, morphogenesis, and pathogenesis under both aerobic and anaerobic condition across various fungal genera. In the dimorphic ascomycete *Candida albicans* (*C. albicans*), knockout of ADH1 significantly impairs hypha formation, resulting in the production of only conidia or short pseudohyphae in liquid media and reduced virulence [8]. Similarly, *ADH1* deficiency in *C. albicans* inhibits hyphal development and mitochondrial oxidative phosphorylation, and lower energy production may lead to delayed trophic development [9]. In *Botrytis cinerea*, conidia from *adh1* knockout mutant strains exhibit altered morphology, lower germination rates and reduced virulence [10]. *T. asahii* is a morphologically and physiologically complex, adaptable yeast-like fungus similar to *C. albicans* [11]. The yeast phase promotes rapid fungal growth and dissemination in circulation, while the hyphal phase facilitates attachment to and penetration of the infected host [12]. Moreover, T. asahii can adhere to and aggregate on implanted hypha devices to form biofilms, leading to persistent infections. Biofilm formation often results in therapeutic failure of antifungal drugs and evasion of the host immune response [13, 14], and it plays a crucial role in both virulence and drug resistance [15].

The alcohol dehydrogenase gene (Gene ID: evm.model.Chr08.320, Gene_symbol: *TaADH_like*) was identified as significantly down-regulated in previous experiments comparing wild-type and fluconazole-resistant strains of *T. asahii* through transcriptomic analyses (BioProject ID: PRJNA941075). In this study, we analyzed the ADH gene family and constructed *TaADH_like* overexpression strains. By comparing the colony morphology, biofilm biomass, stress response, drug resistance, and pathogenicity between the overexpression and wild-type strains, we initially explored the function of *TaADH_like* in *T. asahii*, thereby laying the foundation for further genetic studies of this fungus.

Materials and methods

Strains

The strains used in this study are listed in Table S1. The *T. asahii* YAN0802 (WT) was isolated from giant pandas and cultured in Sabouraud Dextrose Agar (SDA) medium at 28 °C for 3 d.

ADH gene family analysis

ADH gene family members were screened based on previous studies [16]. SMART (http://smart.embl.de/ (accessed on 18 June 2024)) was used to confirm the conserved domains. The phylogenetic trees of ADH were constructed using MEGA-X with maximum likelihood, the WAG + G amino acid model, and 1000 bootstrap replications, visualized by EvolView-v2 (https://evolgenius.info//evolview-v2/ (accessed on 18 June 2024)) [17, 18]. The MEME program (http://alternate.meme-suite.org/tools/meme (accessed on 18 June 2024)) was used to identify conserved motifs in the ADH sequence, with the number of motifs set to 10 and the minimum and maximum widths set to 10 and 50, respectively [19].ADH sequences were compared using MAFFT (https://mafft.cbrc.jp/ (accessed on 18 June 2024)), and TBTools v2.102 was used to visualize the results [20].

Construction of overexpression strains

Total RNA from the WT strain was extracted using the SteadyPure RNA Extraction Kit (Accurate Biotechnology (Hunan) Co., Ltd., Changsha, China) and a cDNA template was synthesized from the RNA via reverse transcription usingEvo M-MLV Plus cDNA Kit (Accurate Biotechnology (Hunan) Co., Ltd., Changsha, China). The DNA of the WT strain was extracted by Rapid Fungi Genomic DNA Isolation Kit (Sangon Biotech, Shanghai, China). The promoter (2000 bp) of the TDH3 gene with high transcriptome expression in the WT strain was selected as the promoter of the target gene *TaADH_like* (accession number PRJNA941075). The cDNA was used as the template to amplify the *TaADH_like* gene, and DNA was used as the template to amplify TDH3_Promoter. The fragments were ligated using the pclone007 Simple Vector Kit (TSINGKE, Beijing, China) and then transferred into *E. coli* Trelief™ 5α strains (TSINGKE, Beijing, China) for amplification [21].

Enzymes QuickCut™ *ASC I* (Yugong, Jiangsu, China) and *Xho I* (Takara, Beijing, China) sheared the pCAMBIA1300ura-GFP-Bar-MCS plasmid, and recombinant plasmids (P1300-HYG-TDH3_Promoter-TaADH_like) were obtained by multifragment recombination with linear plasmids, *TDH3_Promoter*, *TaADH_like*, and *HYG* according to ClonExpress Ultra One Step Cloning Kit (Vazyme, Nanjing, China). Recombinant plasmids were transferred into WT strains by *A. tummefaciens* AGL1 (WEIDI, Shanghai, China) mediated transformation

method [21, 22]. Transformants were screened in SDA containing HYG (300 μg/mL) and cefotaxime sodium (200 μg/mL). PCR and fluorescence observation were used to verify the positive transformants, and RT-qPCR was used to determine the *TaADH_like* expression described previously [16], and the correct strain was named TaADH_like^{OE}. Primers are shown in Table S2.

Determination of the colony growth rate

Individual colonies in the medium were perforated using a 1 cm perforator and then transferred to fresh SDA medium, placed at 28 °C for incubation, and repeated 5 times. The colony diameter was measured daily for 25 consecutive days.

Morphological observation

Morphological differences in conidia and hyphae between the wild-type (WT) and *TaADH_like* overexpression (TaADH_like^{OE}) strains were examined using the copper ring culture method [23]. Conidia were eluted from the SDA medium with PBS buffer, and the concentration of conidia was 1×10^6 CFU/mL with hemocytometer plates. The 5 μL conidial suspension was inoculated into copper ring pores, cultured at 28 °C, and stained with lactophenol cotton blue (Biostime, Qingdao, China) at 4 h, 8 h, 12 h, 16 h, 20 h, 1 d, 3 d, 5 d and 7 d, and observed under a microscope (BX51, Olympus). The length and width of more than 100 conidia from WT and TaADH_like^{OE} strains were measured using ImageJ software.

Fluconazole sensitivity determination

The minimum inhibitory concentration (MIC) of fluconazole for the strains was determined according to the M27-A3 protocol recommended by the Clinical and Laboratory Standards Institute (CLSI) [24]. The MIC was assessed in 96-well plates using a 2-fold serial dilution of fluconazole, resulting in a final drug concentration range of 0.125–64 μg/mL. The inoculum concentration was adjusted to 5×10^5 CFU/mL and 100 μL was added to each well. Plates were incubated for 48 h at 200 rpm/min at 28 °C. Each experiment was performed in triplicate.

Comparison of spot tests for susceptibility of WT and TaADH_like^{OE} strains to fluconazole inhibitory concentrations. SDA medium containing different concentrations of fluconazole (0, 2, 8, 16, 32, 64, 128, 256 μg/mL) was prepared. For each fluconazole concentration, 2 μL of conidial suspensions at 1×10^7 CFU/mL, 1×10^6 CFU/mL, and 1×10^5 CFU/mL were spotted onto the respective SDA medium, incubated at 28℃ and observed after 48 h, with a 50% reduction of colonies as the observation threshold. Each experiment was performed in triplicate.

Stress experiment

SDA medium containing 0.2 mM $CoCl_2$, SDS (0.004% W/V), CR (0.4 mg/mL and 1 mg/mL), 1.5 M NaCl, and 2 M sorbitol were prepared, respectively. Inoculate 2 μL of each concentration of conidial suspension 1×10^7 CFU/mL, 1×10^6 CFU/mL and 1×10^5 CFU/mL in medium and incubate at 28 ℃ for 3 d. The phenotypic differences between the strains were observed daily. The results were repeated three times.

Acetaldehyde content detection

The acetaldehyde content of the strains was determined using High Performance Liquid Chromatography (HPLC) (1260 infinityII, Agilent). Equal masses of WT and TaADH_like^{OE} strains were ground, and perchloric acid and sodium acetate were added in a volume twice that of the sample to adjust the pH to 4.0. The supernatant was transferred to a pre-cooled centrifuge tube, and an equal volume of DNPH (Aladdin, Shanghai, China) was added and shaken for 1 h. Subsequently, acetonitrile was added in a volume twice that of the sample and mixed by shaking for 30 min. The supernatant was spun dry in a rotary evaporator, and 2 mL of acetonitrile was dissolved for detection. The mobile phase was composed of 50% acetonitrile and 50% water, with a flow rate of 1 mL/min. The C18 solid phase extraction column was used, with a column temperature set at 30 °C and an injection volume of 20 μL. The results were repeated three times.

Determination of biofilm biomass

The quantification of biofilm biomass using the XTT reduction method was performed as previously described [25]. Each 96-well cell culture plate was added with 100 μL conidial suspension (1×10^6 CFU/mL), incubated at 28℃ for 2 h, lightly washed twice with PBS, and then re-added with 100 μL fresh SDB culture medium at 28℃. The culture medium was changed every 24 h. At 24, 48, and 72 h, the 96-well plates were removed, washed three times with PBS, and 200 μL of XTT-menadione solution was added to each well, and incubated at 28℃ for 4 h in the dark. Using 100 μL of liquid per well in a new 96-well plate, absorbance was measured at 492 nm (Varioskan Fish, Thermo). Each experiment was performed in triplicate.

ROS assay

The final concentration of 1 mg/mL Dihydroethidium (Beijing Solarbio Science & Technology Co., Ltd., China) 10 μL and 1 mL of conidial suspension (1×10^7 CFU/mL) were mixed thoroughly, incubated for 30 min at 37 ℃ in the dark, and then 200 μL of suspension was added into a black 96-well plate, and the fluorescence intensity (excitation wavelength of 518 nm, emission wavelength of 610 nm) was measured (Varioskan Fish, Thermo).The

results were repeated three times. Meanwhile, 10 μL of suspension were aspirated to observe the fluorescence of the strain (BX51, Olympus).

Pathogenicity experiment

Animal

Eight-week-old female ICR mice (SPF(BEIJING)BIOTECHNOLOGY CO.,LTD., China) were immunosuppressed with 80 mg/kg cyclophosphamide and 25,000 units of penicillin sodium four days prior to the experiment. The mice were divided into three groups, A, B and C. Groups A and B were inoculated with 0.1 mL of 1×10^7 CFU/mL conidial suspensions of the WT and TaADH_like^{OE} strains, respectively, via the tail vein. Group C served as the control, inoculated with 0.1 mL of saline via the tail vein. The mice were fed and watered ad libitum, weighed at 1 d intervals, and recorded the survival rate.

Tissue fungal burden analysis

Mice in groups A and B were euthanized by cervical dislocation on 1, 3, 5 and 7 d (5 biological replicates), and heart, liver, spleen, lung, and kidney tissue fungal burden were determined by plate colony counting. Mouse hearts, livers, spleens, lungs, and kidneys were aseptically isolated, ground, and rinsed into sterile EP tubes with 2 mL of saline. Tissue solutions were diluted at 10^{-1}, 10^{-2}, and 10^{-3} multiplicities, and 100 μL of each concentration was uniformly spread in SDA medium (3 replicates) and placed at 28 °C for 2–4 d. Colonies on the plates were counted, and the amount of fungal burden in the tissues was calculated. The fungal burden per gram of tissue was expressed as log (CFU/g), using the formula:

Fungal burden = $\log[X/(A/2 \times 10^{-n} \times 0.1)]$ [log(CFU/g)]

[X: number of colonies per plate count (CFU); A: mass of tissue organs (g); 10^{-n}: dilution ratio; 2; volume of normal saline used in elution tissue (mL); 0.1: volume of suspended fluid used in inoculation plate (mL)]

Histopathological

Mice in groups A and B were euthanized by cervical dislocation on 1, 3, 5 and 7 d (5 biological replicates), and tissues of heart, liver, spleen, lungs and kidneys were removed and fixed in 4% paraformaldehyde for 24 h. They were routinely dehydrated and dipped in wax, embedded and sectioned, and then stained by Hematoxylin-Eosin staining (HE) and peroxodioic acid-Schiff staining (PAS), respectively.

RT-qPCR analysis

The strains were grown in Sabouraud Dextrose Broth (SDB) medium at 28 °C for 3 d at 200 rpm/min. RT-qPCR methods were as described previously [16]. WT and TaADH_like^{OE} strains total RNA was extracted and reverse transcribed to cDNA and 18sRNA was used as an internal reference for RT-qPCR assay. Primers are shown in Table S3-S5.

Data statistics

GraphPad Prism 9.5 was used to calculate the mean and standard deviation. Tissue fungal burden statistics were analyzed using a two-way ANOVA and all other tests were analyzed by a t-test using the Holm-Šídák method. **** $P < 0.0001$, *** $P < 0.001$, ** $P < 0.01$, * $P < 0.05$.

Results

ADH gene family analysis

To understand the genetic evolutionary relationships of the alcohol dehydrogenase (ADH) gene family in *T. asahii*, comparative analysis of the ADH gene families in *C. albicans* and *S. cerevisiae* was conducted. Seventeen members of the ADH gene family containing both ADH_N and ADH_Zinc_N domains were identified, including six genes from *T. asahii*, six from *S. cerevisiae*, and five from *C. albicans*, which were labelled according to the genome annotations. The phylogenetic evolutionary tree divides 17 genes into three groups (Fig. 1-I). The predicted protein lengths encoded by the *ADH* genes ranged from 282 to 381 amino acids (aa). The molecular weights ranged from 30935.4 Da (CaADH3) to 40586.6 Da (CaFADH). The isoelectric point values of these TaADHs ranged from 5.58 to 8.65 and included 3 basic and 14 acidic proteins (Table 1).

The Zinc 1 binding motif, Zinc 2 binding motif and NADPH binding motif are important binding motifs for ADH. The Zinc 1 binding motif [GHE(x)2G(X)5G(X)2 V] contains catalytic zinc amino acid coordination residues. The Zinc 2 binding motif [GD(X) 9,10 C(X)2 C(X)2 C(X)7 C] contains structural zinc amino acid coordination residues (Fig. 1-III). The NADPH binding motif [GXG(X)2G] is highly conserved among ADH members (Fig. 1-III). The genes with higher homology have similar protein motif compositions. Motif1 and motif7 are unique to group B. Similarly, motif5 is a significant motif in groups A and B but absent in group C. All members of groups A and B, along with *TaADH_like*, contain motif3 and motif4, which may be the characteristic motifs of alcohol dehydrogenase (Fig. 1-IVA). The number of CDS regions varies from 1 to 6 across groups A-C. In *C. albicans* and *S. cerevisiae*, only *CaFADH* has two CDS regions, whereas the others have one CDS region, but all *TaADH* possess multiple CDS regions (Fig. 1-IVB).

Transformant verification

The transformant was observed to green fluorescens in the dark field (Figure S1-I), and PCR amplification yielded a 4500 bp HYG-TDH3_Promoter-TaADH_like target band (Figure S1-II), with the mRNA level of

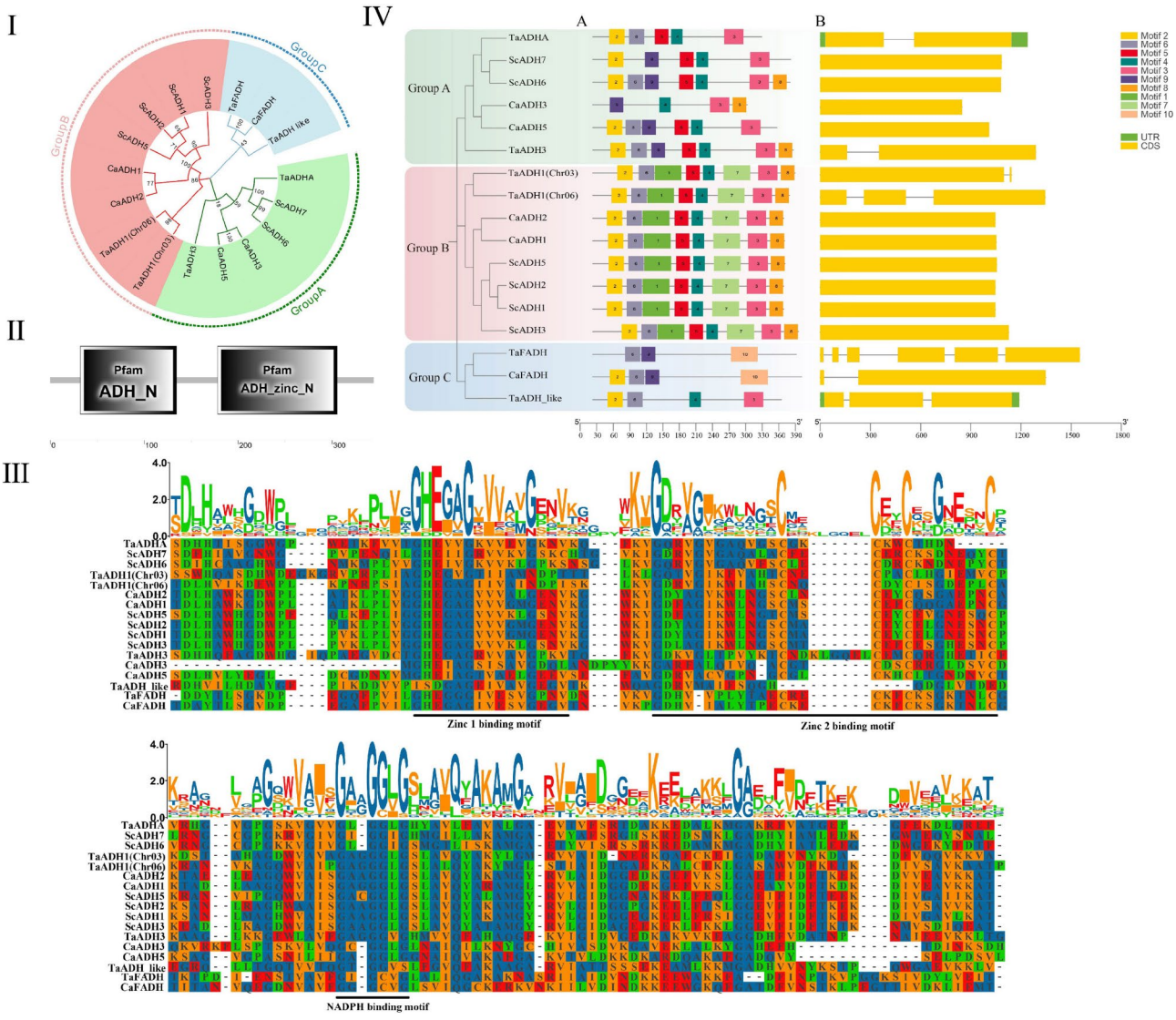

Fig. 1 ADH gene family analysis. I, Phylogenetic analysis of the *T. asahii*, *C. albicans* and *S. cerevisiae* ADH gene family members. II, *TaADH_like* domain diagram. III, Partial results of amino acid sequence alignment of 17 *ADH* genes. IV, Phylogenetic tree, gene structure and conserved motifs of ADHs. A, Phylogenetic tree and motif analysis. B, Gene structure analysis of *ADHs*

TaADH_like about 59-fold higher than WT ($P<0.0001$) (Figure S1-III). In conclusion, the *TaADH_like* overexpression strain was successfully constructed and named TaADH_like^{OE} strain.

Overexpression of *TaADH_like* decreased the germination and growth rate of *T. asahii*

TaADH_like^{OE} and WT were cultured on SDA medium for 25 days. WT exhibited significantly faster growth than TaADH_like^{OE} ($P<0.0001$), with growth plateauing after 21 days (Fig. 2-I). Microscopic observations revealed differences in germination between TaADH_like^{OE} and WT (Fig. 2-II). Both TaADH_like^{OE} and WT conidia began to germinate at 4 h (Fig. 2-II A and a). At 8 h, WT conidia elongated and were significantly longer than TaADH_like^{OE} (Fig. 2-II B and b). At 12 h, TaADH_like^{OE} conidia were willow-like, and WT conidia developed septa and formed short hyphae (Fig. 2-II C and c). At 16 h, TaADH_like^{OE} willow-like conidia appeared septa, and a large number of conidia were still germinating. WT short hyphae with increased septa in the middle formed rectangular conidia (Fig. 2-II D and d). At 20 h, TaADH_like^{OE} was still germinating, WT conidia increased, and rectangular conidia gradually became round (Fig. 2-II E and e). In conclusion, TaADH_like^{OE} germinated slower than WT, consistent with the growth curve results. The length and width of over 100 conidia of both TaADH_like^{OE} and WT were measured, and the results showed that WT conidia tended to round while TaADH_like^{OE} conidia tended to oval (Fig. 2-III). The

Table 1 Detailed information of the ADH family members identified

Gene_symbol	Gene ID	Length	MW(Da)	PI
TaADHA	evm.model.Chr02.955	308	32819.7	7.39
TaADH1(Chr3)	evm.model.Chr03.1119	369	39170.8	7.19
TaFADH	evm.model.Chr04.188	371	39685.2	6.50
TaADH1(Chr6)	evm.model.Chr06.247	359	38170.5	5.74
TaADH_like	evm.model.Chr08.320	344	36829.0	6.96
TaADH3	evm.model.Chr08.391	366	38786.3	6.18
CaADH2	C1_08330C_A-T-p1	348	36807.2	6.26
CaADH3	C2_04470W_A-T-p1	282	30935.4	6.24
CaADH1	C5_05050W_A-T-p1	350	36909.3	5.85
CaADH5	CR_02070C_A-T-p1	336	35702.7	5.58
CaFADH	CR_10250C_A-T-p1	381	40586.6	5.96
ScADH5	YBR145W	351	37648.1	5.94
ScADH7	YCR105W	361	39348.4	6.91
ScADH3	YMR083W	375	40369.5	8.65
ScADH2	YMR303C	348	36731.9	6.26
ScADH6	YMR318C	360	39617.5	6.28
ScADH1	YOL086C	348	36849.1	6.21

genes related to WT and TaADH_like^{OE} conidia were analyzed by RT-qPCR. The results indicated that genes associated with conidial development and maturation (*apsA*, *umv1*, *vosA*, *DIT1*, and *fim1*) were significantly down-regulated (Fig. 2-IV). These changes may have contributed to the altered conidial morphology and slower growth observed following *TaADH_like* overexpression.

Overexpression of *TaADH_like* mediates *T. asahii* dimorphic transition

The morphology of TaADH_like^{OE} and WT showed obvious differences on SDA (Fig. 3-I). TaADH_like^{OE} colonies appeared small, creamy-white, and lustrous, with irregular growth and a moist surface characterized by prominent brain-like folds. In contrast, WT colonies are large, white and translucent, with neat radial outward growth at the edges, dry surface, and few downy folds.

The morphology differences were observed by microscope (Fig. 3-II). On Day 1, both TaADH_like^{OE} and WT strains showed a large number of conidia (Fig. 3-II A and a). On Day 3, TaADH_like^{OE} conidia had elongated, with the majority undergoing germination, while WT exhibited long chains of pseudohyphae and arthroconidia (Fig. 3-II B and b). On day 5, TaADH_like^{OE} conidia were mostly fusiform with large vacuoles in the middle, with many conidia linked together in clusters. WT displayed hyphae, accompanied by numerous pseudohyphae and arthroconidia, the conidia were mostly round (Fig. 3-II C and c). On Day 7, TaADH_like^{OE} had a large number of oval conidia and pseudohyphae, while WT showed elongated hyphae (Fig. 3-II D and d). These observations indicate that overexpression of *TaADH_like* caused *T. asahii* to transition from the hyphal phase to the yeast phase.

The genes related to WT and TaADH_like^{OE} hyphae were analyzed by RT-qPCR. *BRG1*, *Ras1*, *Rac1*, *Rho1*, *CDC42* and *cmkA* genes related to hyphae growth, development and regulation were significantly down-regulated, and the *NRG1* and *RGF1* genes encoding hypha deterrent proteins were significantly up-regulated (Fig. 3-III). This coordinated regulation drove the transition of *T. asahii* from the hyphal phase to the yeast phase.

Slightly reduced fluconazole sensitivity

In the spot test, the concentration at which colony growth was reduced by 50% was 2 μg/mL for WT and 8 μg/mL for TaADH_like^{OE} (Fig. 4). In the MIC assay, the MIC values were approximately 4 μg/mL for WT and 8 μg/mL for TaADH_like^{OE} (Table 2). Due to the morphological characteristics of WT, some white floating colonies appeared in liquid culture, which caused discrepancies between the results and those of the spot test. Overall, *TaADH_like* overexpression led to a slight increase in resistance to *T. asahii.*

Stress experiment

$CoCl_2$ is a chemical hypoxia mimetic in eukaryotic cells [26]. Compared to TaADH_like^{OE}, WT inoculated with 1×10^6 and 1×10^5 CFU/mL conidial suspensions on SDA exhibited significant inhibition (Fig. 5-I). This suggests that overexpression of *TaADH_like* reduces the sensitivity under hypoxic conditions. The integrity of the cell wall was assessed using cell wall disruptors sodium lauryl sulfate (SDS) and Congo red (CR) (Fig. 5-II). There was no significant difference in the growth of all tested strains, indicating that overexpression of *TaADH_like* did not affect the integrity of *T. asahii* cell wall. Additionally, it was found that WT growth was progressively inhibited with increasing CR concentration, primarily in the form of reduced radial hyphal growth. In contrast, TaADH_like^{OE} exhibited a yeast phase, and its growth was unaffected by CR concentration.

TaADH_like^{OE} exhibited significant suppression on SDA medium containing the osmotic stressors sorbitol and NaCl (Fig. 5-III). The expression of genes related to osmotic pressure regulation was analyzed by RT-qPCR (Fig. 5-IV). Following *TaADH_like* overexpression, genes associated with the osmolarity-related *Sho1* and *CnNIK1* (*Sln1*)-regulated HOG1 pathways were dysregulated. The *Sho1* gene was most significantly downregulated, while the *CnNIK1* gene was significantly upregulated. The *Ste11* gene showed no differential expression, and the remaining genes in the regulatory pathway were downregulated. Overexpression of *TaADH_like* inhibited the Sho1 pathway, thereby enhancing the osmotic stress sensitivity of *T. asahii*, while the CnNIK1 pathway compensated for the Sho1 pathway.

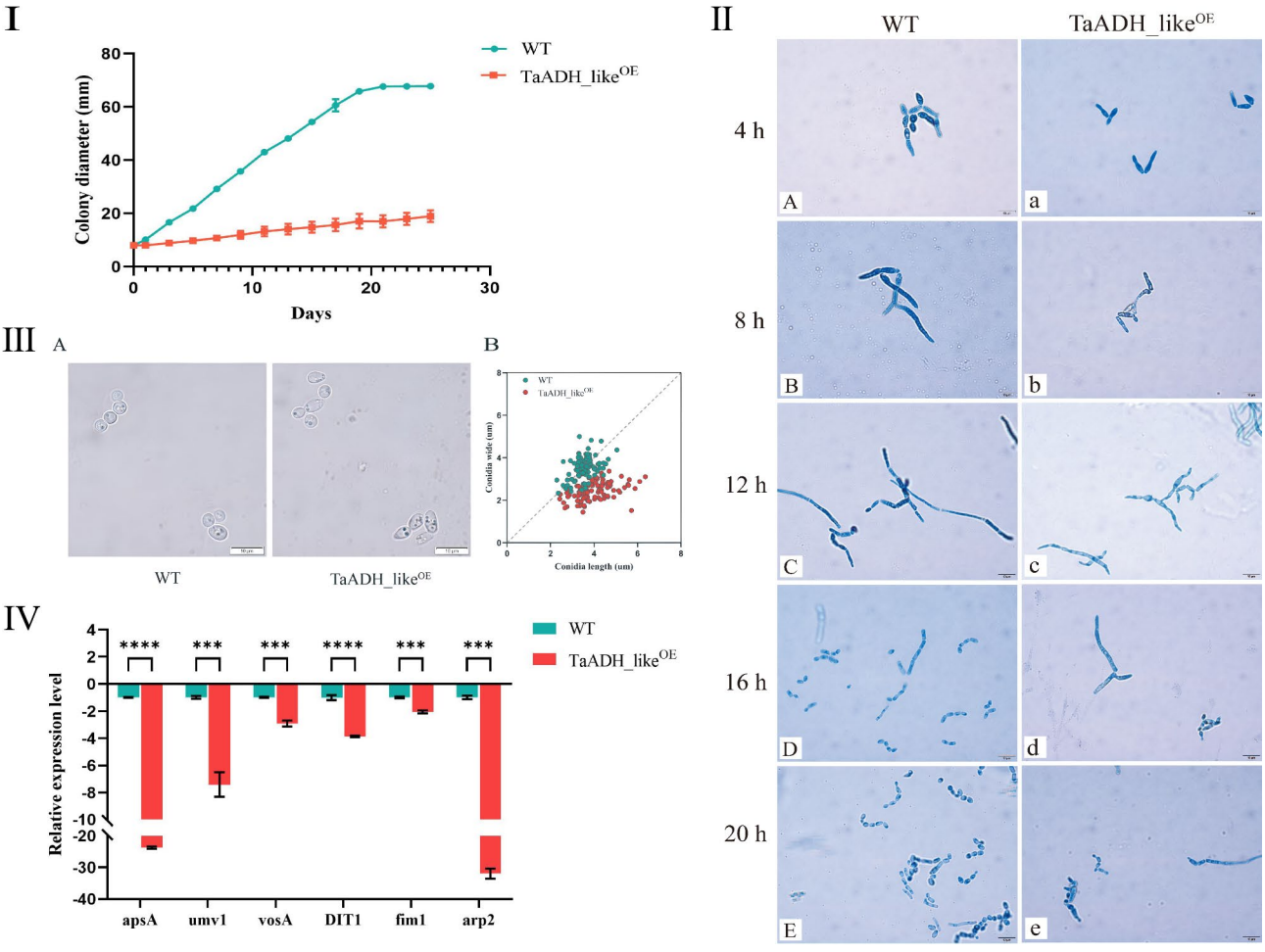

Fig. 2 Overexpression of *TaADH_like* decreased the germination and growth rate of *T. asahii*. I, Growth curve of TaADH_like^{OE} and WT. Results are expressed as mean ± SD. II, Microscopic observation on the growth difference between TaADH_like^{OE} and WT during germination. Scale, 10 μm. III, WT and TaADH_like^{OE} ratio of conidia length to width, Scale, 10 μm. IV, RT-qPCR analysis of regulating conidia-related genes. Positive and negative represent up- and down-regulation, and expression level is expressed as $2^{|-\Delta\Delta Ct|}$

Acetaldehyde content and biofilm metabolic activity determination

Acetaldehyde, a toxic volatile organic compound with an irritating odor, was quantified by HPLC after being derivatized with 2,4-dinitrophenylhydrazine (DNPH) to form stable hydrazone compounds [27]. The regression equation of the standard curve was y=26005x + 4.047 (R^2 = 0.9993, y = peak area, x = acetaldehyde-DNPH content). The acetaldehyde-DNPH content of the 20 μL sample volume of WT and TaADH_like^{OE} was 0.0081 μg and 0.0125 μg, respectively (Fig. 6-I). The overexpression of the *TaADH_like* increased acetaldehyde accumulation in *T. asahii*, potentially implicating its role in the interconversion between alcohols and aldehydes.

The biofilm metabolic activity of TaADH_like^{OE} was significantly higher than that of WT at 24, 48, and 72 h. The biofilm metabolic activity of TaADH_like^{OE} peaked at 48 h and maintained until 72 h (Fig. 6-II). Overexpression of *TaADH_like* enhanced biofilm metabolic activity in *T. asahii*.

ROS determination

Dihydroethidium (DHE) is a widely used cell-permeable fluorescent probe for detecting superoxide anion (O_2^-) radicals [28]. When the level of superoxide anions inside the cell is high, more Ethidium is generated, resulting in stronger red fluorescence. At the same exposure time, the intensity of red fluorescence observed for TaADH_like^{OE} was significantly weaker than that of WT under the microscope (Fig. 7-I). Fluorescence intensity measurements revealed that TaADH_like^{OE} produced significantly lower fluorescence than WT ($P < 0.001$), consistent with the microscopic observations (Fig. 7-II).

Pathogenicity

Mice inoculated with WT appeared to die on 1 d and experienced a significant mortality spike on 3 d, dropping

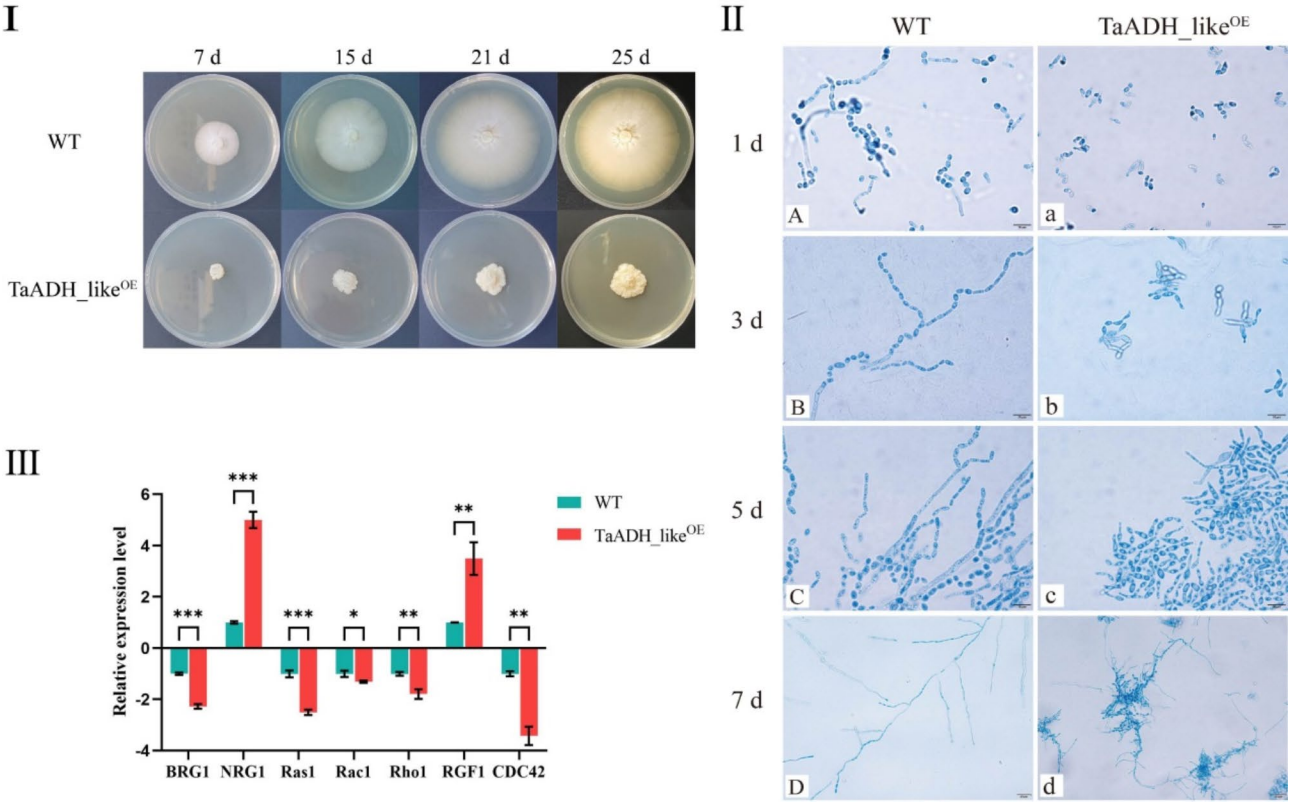

Fig. 3 Overexpression of *TaADH_like* mediates *T. asahii* hyphae-to-yeast conversion. I, Colony morphology of WT and TaADH_like^{OE}. II, Morphology of conidia and hypha of WT and TaADH_like^{OE}. A-C and a-c scales are 10 μm, and D and d scales are 20 μm. III, RT-qPCR analysis of regulating hypha-related genes. Positive and negative represent up- and down-regulation, and an expression level is expressed as $2^{|-\Delta\Delta Ct|}$

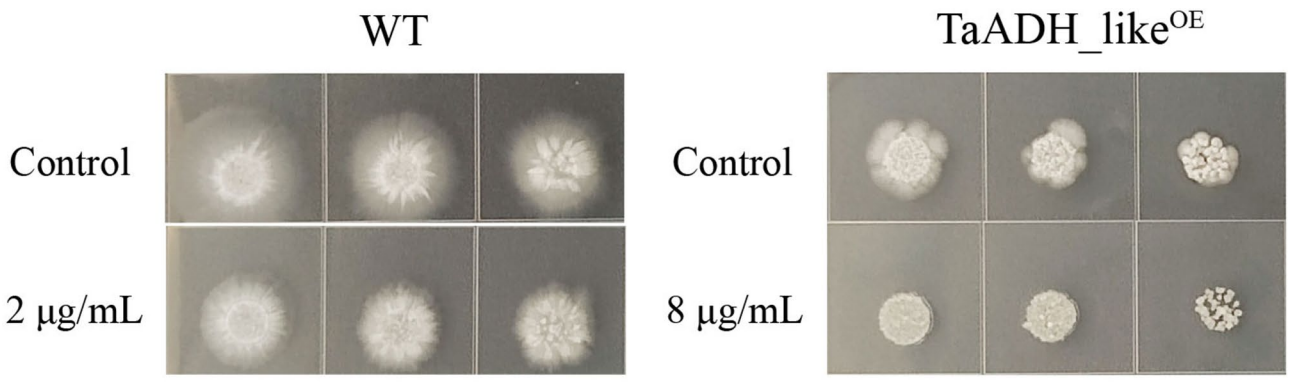

Fig. 4 Fluconazole sensitivity determination of WT and TaADH_like^{OE}. The conidia concentration from left to right of the colony was 1×10^7, 1×10^6 and 1×10^5 CFU/mL

Table 2 The minimum inhibitory concentration (MIC) was determined

Strain	MIC Value
WT	4 μg/mL
TaADH_like^{OE}	8 μg/mL

the survival rate to less than 30%. In contrast, mice inoculated with TaADH_like^{OE} exhibited a slower rate of death and maintained a survival rate above 50% within 7 days (Fig. 8-I). Additionally, mice inoculated with WT and TaADH_like^{OE} showed a significant decrease in body weight compared to control mice (Fig. 8-II). Due to the high mortality of WT-inoculated mice within 3 days, the remaining number of mice was insufficient to continue the body weight change test, and thus only the body weight changes within the first 3 days were recorded. Overall, overexpression of *TaADH_like* reduced the lethality of *T. asahii* in mice.

The results of tissue fungal broaden analysis are shown in Fig. 8-III. The tissue fungal burden in mice inoculated

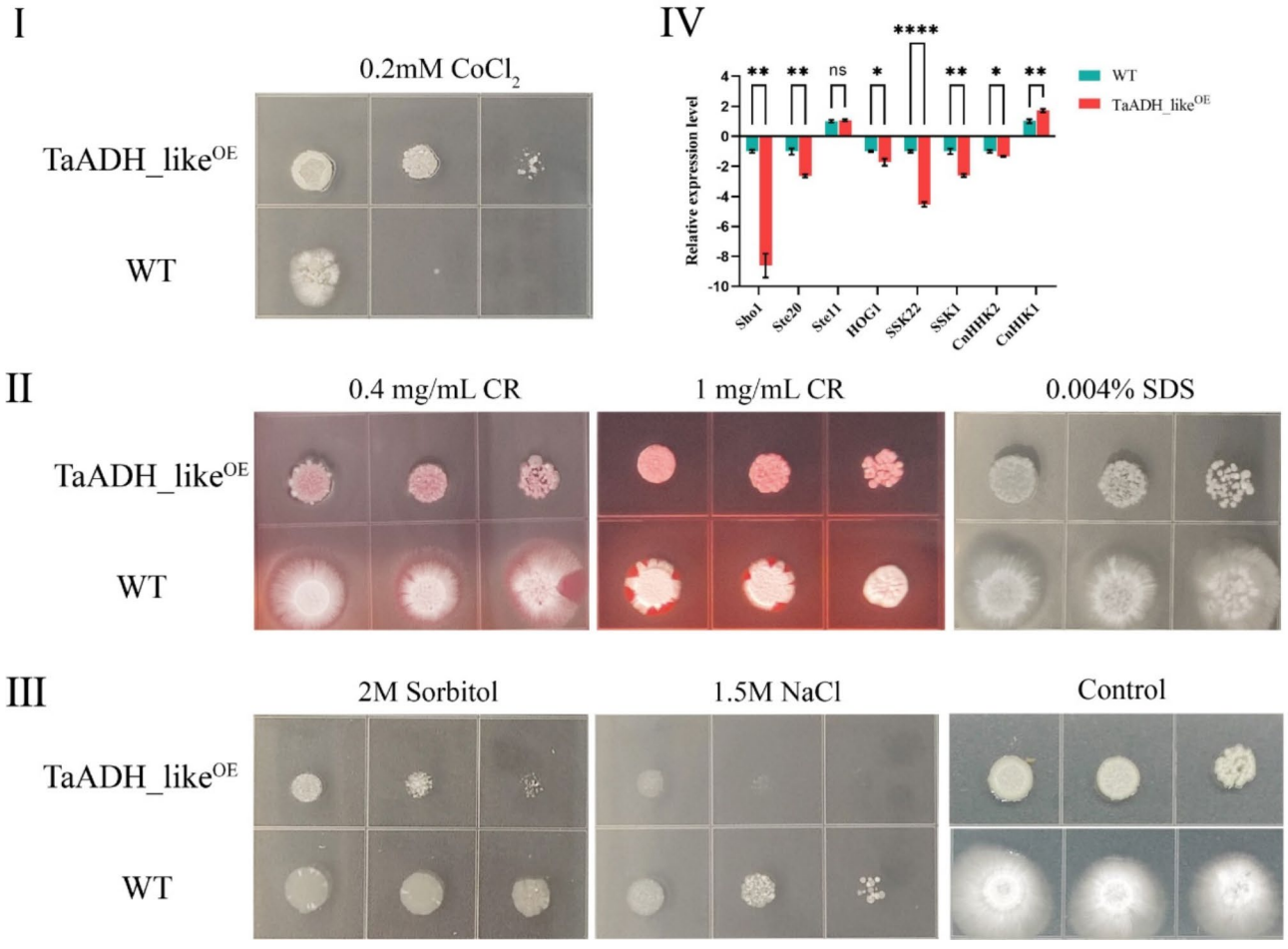

Fig. 5 Stress experiment. I, II and III were WT and TaADH_like^{OE} hypoxia, cell wall inhibitor and osmotic stress experiments, respectively. Control The conidia concentration from left to right of the colony was 1×10^7, 1×10^6 and 1×10^5 CFU/mL. IV, RT-qPCR analysis of regulating osmotic stress related genes. Positive and negative represent up- and down-regulation, and expression level is expressed as $2^{|-\Delta\Delta Ct|}$

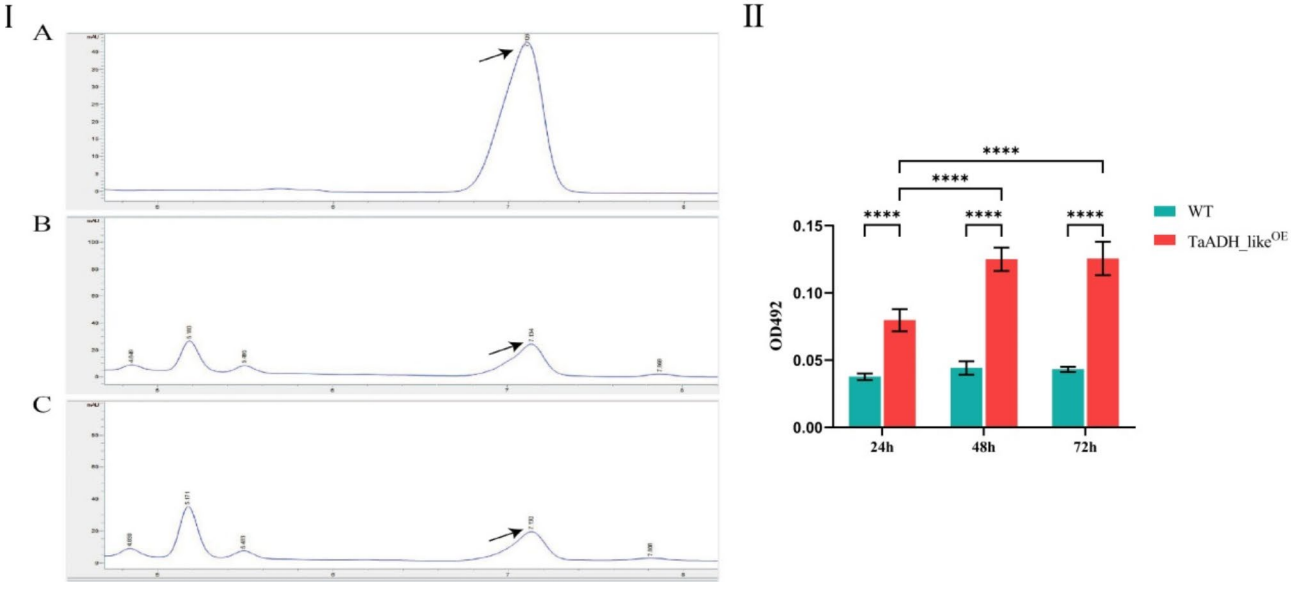

Fig. 6 Acetaldehyde content and biofilm metabolic activity determination. I, liquid chromatogram. **A**, **B** and C are chromatograms of acetaldehyde-DNPH standard, TaADH_like^{OE} and WT, respectively. II, WT and TaADH_like^{OE} biofilm metabolic activity assay

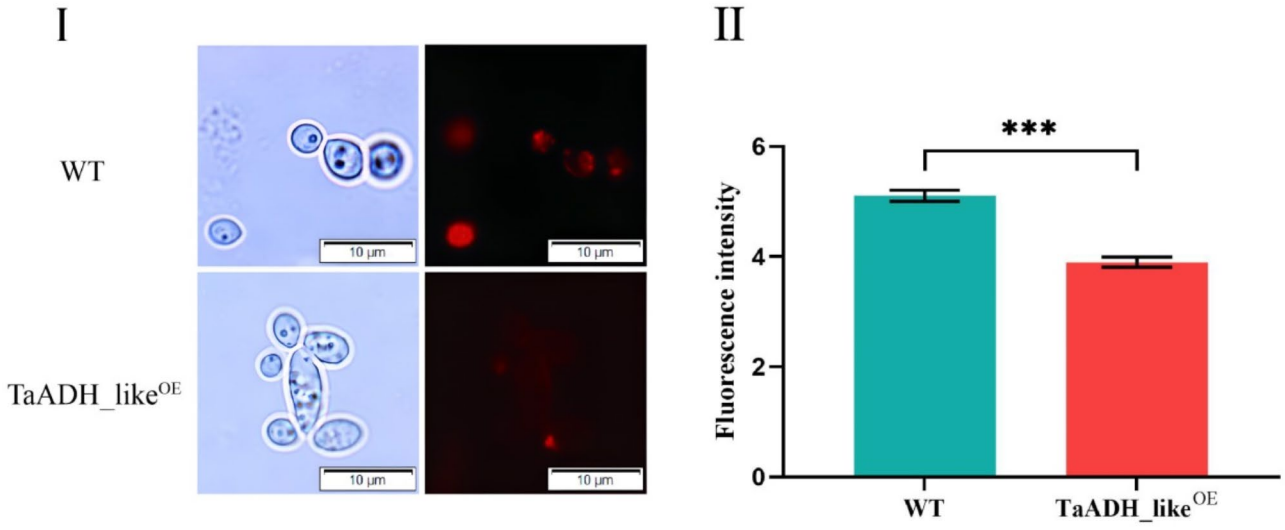

Fig. 7 WT and TaADH_like^{OE} ROS were detected. I, Microscopic observation of TaADH_like^{OE} and WT red fluorescence. Scale, 10 μm. II, Fluorescence intensity measurements for TaADH_like^{OE} and WT

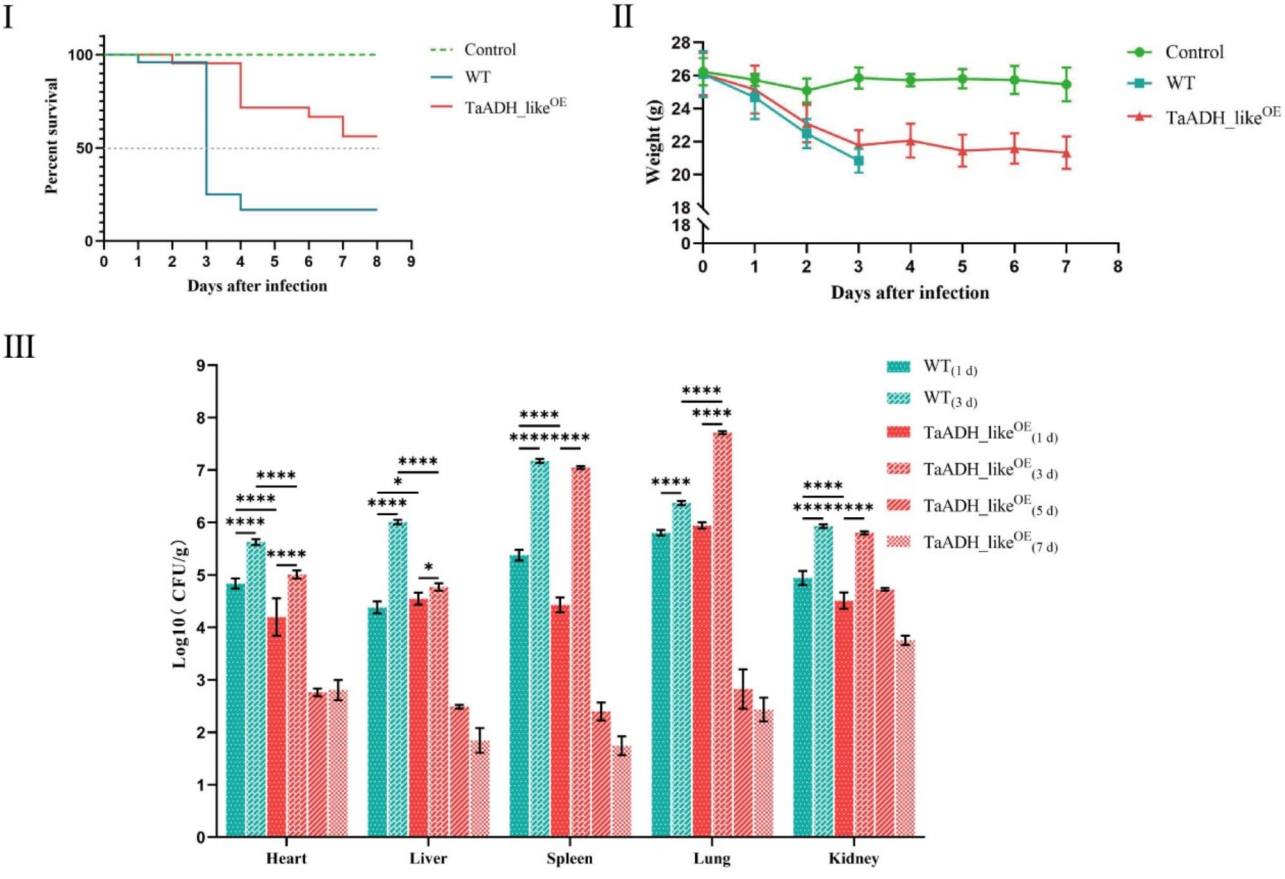

Fig. 8 Percent survival, weight and tissue fungal broaden analysis in mice inoculated with WT and TaADH_like^{OE} strains. I and II are WT and TaADH_like^{OE} survival and weight change, respectively. III, WT and TaADH_like^{OE} tissue fungal burden

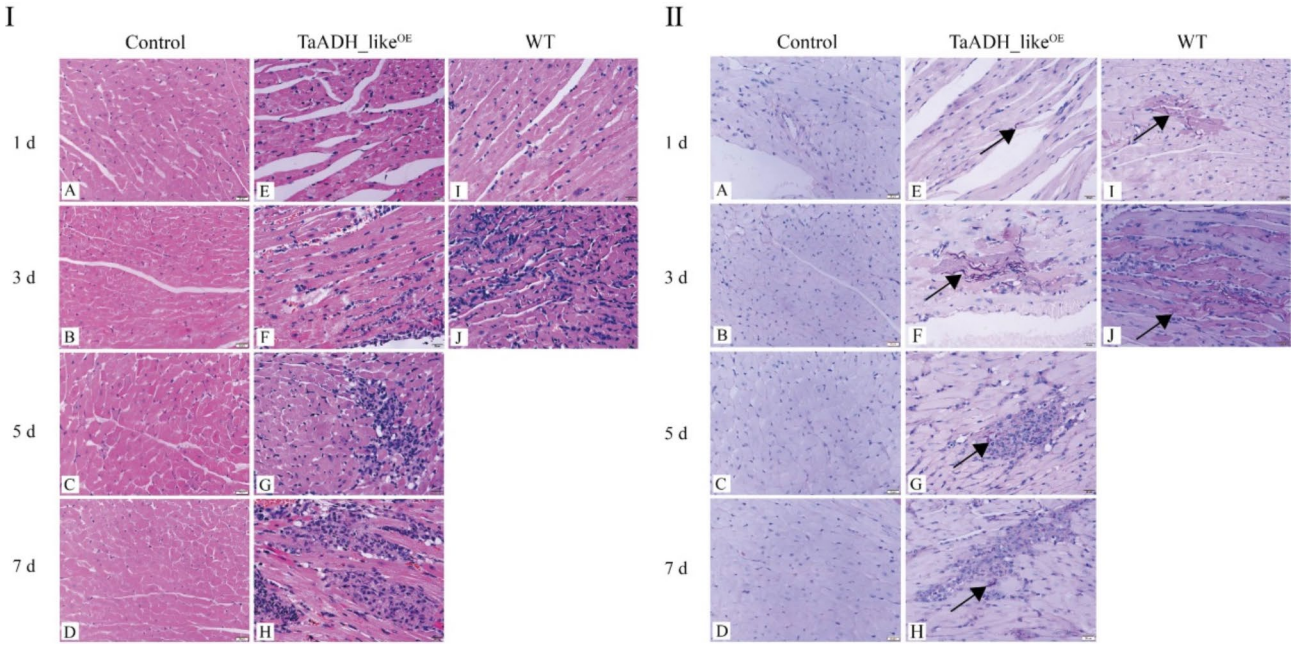

Fig. 9 HE and PAS staining of heart tissue from mice infected with WT and TaADH_like^{OE}. I, HE staining of heart tissue. II, PAS staining of heart tissue. Representative HE and PAS stained sections of heart tissues 1–7 d and 1–3 d after infection of mice by control (A-D), TaADH_like^{OE} (E-H) and WT (I and J), respectively. Scale bar, 20 μm. Black arrows point to conidia or hyphae

with WT and TaADH_like^{OE} peaked at 3 d, which was significantly higher than that at 1 d ($P < 0.0001$). Subsequently, a decreasing trend was observed in the fungal burden of mice inoculated with TaADH_like^{OE}. On Day 1, the fungal burden in the heart, spleen, and kidney tissues of WT-inoculated mice was significantly higher ($P < 0.0001$) than that in TaADH_like^{OE}-inoculated mice. On Day 3, the fungal burden in the lung tissues of TaADH_like^{OE}-inoculated mice was significantly higher than that in WT-inoculated mice ($P < 0.0001$), while the remaining tissues exhibited lower burdens compared to WT-inoculated mice. Overall, WT colonised tissues stronger than the TaADH_like^{OE} strain.

Histopathological

Pathological histology showed that WT-inoculated mice developed pathological damage earlier and exhibited more severe damage compared to TaADH_like^{OE}-inoculated mice. The TaADH_like^{OE}-inoculated mice showed infiltration of inflammatory cells between myocardial fibres on 3 d, and myocardial fibre lysis and rupture on 5 and 7 d, with an increase in inflammatory cells, which were similar to the results of the WT-inoculated mice on 3 d (Fig. 9-I). There were no obvious abnormalities in the liver tissues of TaADH_like^{OE}-inoculated mice on 1 d, and the cytoplasmal structure of some hepatocytes was damaged on 3 d, which was similar to WT-inoculated mice on 1 d. In both WT- and TaADH_like^{OE}-inoculated mice, the central vein and sinusoid space were enlarged and the lumen was filled with red blood cells on 3 and 5 d, respectively (Figure S2-I). The spleen tissues from WT-inoculated mice showed splenic pulp congestion at 1–3 d, with obvious connective tissue hyperplasia and thickened splenic trabeculae, leading to fibrosis (Figure S3-I). The kidney tissues from both WT- and TaADH_like^{OE}-inoculated mice exhibited adhesion of the renal capsule to the vascular balloon and occlusion of the balloon lumen on 1 and 3 d, respectively (Figure S4-I). However, the WT- and TaADH_like^{OE}-inoculated mice showed similar levels of damage in lung tissues (Figure S5-I).

All tissues exhibited the highest levels of conidial or hyphal infections on 3 d, which is consistent with the tissue fungal burden results (Fig. 9-II, S2-II, S3-II, S4-II, and S5-II). In the WT-inoculated mice, kidneys showed an elongated hyphal state on 3 d (Figure S4-II). No conidia were detected in the liver and spleen of the TaADH_like^{OE}-inoculated mice on 1 d (Figure S2-II and Figure S3-II). The higher tissue fungal burden in lung tissues of the TaADH_like^{OE}-inoculated mice on 3 d compared to the WT-inoculated mice. This may be due to the overexpression of *TaADH_like*, which caused the transition of *T. asahii* from the hyphal phase to the yeast phase. This shift may have altered the strain's preference for tissue colonization, leading to a similar degree of pathological damage in lung tissues of WT- and TaADH_like^{OE}-inoculated mice after 3 d.

Discussion

Trichosporon asahii is an important pathogenic fungus for humans and animals, and the study of gene function is a crucial research tool for exploring its drug resistance and pathogenicity. In this study, we conducted a preliminary investigation into the function of the *TaADH_like* gene in *T. asahii*, which lays the foundation for in-depth research on the mechanism of drug resistance and pathogenicity of *T. asahii*.

ADH gene family analysis

S. cerevisiae and *C. albicans* serve as model fungi, with *C. albicans* being a common pathogenic fungus in humans and animals [29, 30]. These two model fungi were selected to investigate the genetic evolutionary relationships of *ADH* in *T.asahii*. S-(hydroxymethyl) glutathione dehydrogenase (FADH), considered the progenitor of the ADH gene family, together with alcohol dehydrogenase, constitutes the ADH gene family [31]. In this study, TaADH_like clusters with FADH in the phylogenetic tree. This may be because TaADH_like lacks motif5 of groups A and B, and is also deficient in group B - specific motif1 and motif7. Motif3 and motif 4 are present in both groups A and B, as well as in TaADH_like, and may be characteristic of alcohol dehydrogenase. However, sequence alignment results indicate significant differences between TaADH_like and other alcohol dehydrogenases. This may explain why TaADH_like is annotated as zinc-type alcohol dehydrogenase-like rather than alcohol dehydrogenase, and is not clustered with groups A and B. TaADH_like may be intermediate between FADH and alcohol dehydrogenase, but its correlation remains unclear. Most ADHs in *C. albicans* and *S. cerevisiae* possess a single CDS region, whereas *T. asahii* typically contains multiple CDS regions. The simpler gene structure of the saccharomycota (*S. cerevisiae* and *C. albicans*) has also been found in the Cyclophilin family [32]. *C. albicans* and *S. cerevisiae* exhibit higher homology than *T. asahii*. Although the basidiomycota (*T. asahii*) and the saccharomycota (*S. cerevisiae* and *C. albicans*) are genetically distinct in gene structure, the types and distribution of motifs are similar in the same group.

The overexpression of *TaADH_like* mediates the dimorphic transition in *T. asahii*

Dimorphic transitions are crucial for fungal growth. *T. asahii*, a morphologically and physiologically complex dimorphic fungus, can grow as yeast or exhibit filamentous growth, forming pseudohyphae and hyphae with abundant articulated conidia, similar to *C. albicans* [11]. In this study, overexpression of *TaADH_like* resulted in reduced hyphae formation, slowed conidia germination, and an arthroconidia formation of pseudohyphae, similar to the results after *ADH1* gene knockdown in *C. albicans* [8], where *TaADH_like* exerted an opposing regulatory effect to the *ADH1*. In *Aspergillus nidulans*, *vosA* regulates conidial growth and development, promoting their maturation and germination [33]. Similarly, *umv1* fulfills a comparable regulatory role in *Ustilago maydis* [34]. In *Schizosaccharomyces pombe*, *fim1* is involved in sexual reproduction with conidia [35], whereas *apsA* is involved in asexual development in *Aspergillus nidulans* [36]. *DIT1* encodes a spore wall maturation protein in yeast [37], and *Arp2* is essential for the hydrophobin protein on the conidial surface in *Aspergillus fumigatus* [38]. Together, these genes regulate conidia growth and development, and *TaADH_like* overexpression reduced the expression of these genes, resulting in slower conidia germination in TaADH_like^{OE}.

Additionally, genes associated with hyphal growth, development, and regulation—*BRG1*, *Ras1*, *Rac1*, *Rho1*, *CDC42*, and *cmkA*—were significantly down-regulated in TaADH_like^{OE}, while the hyphal deterrent proteins *NRG1* and *RGF1* were significantly up-regulated. *BRG1* encodes a DNA-binding protein that serves as a key regulator of fungal morphology. In *C. albicans*, mutants lacking *BRG1* grew as yeast under all tested conditions, whereas overexpression of *BRG1* promoted hyphal growth [39]. *NRG1* encodes a hyphae deterrent protein that represses hyphae formation and hyphae-associated gene expression [40]. Nrg1p and Rfg1p are transcription factors that negatively regulate hyphal formation. Reducing *Nrg1* transcript levels enhances hyphal growth and hyphae-specific gene expression, and overexpression of *RGF1* drives pseudohyphae formation under yeast growth conditions [41, 42]. The Rho-related GTPase family is also plays a crucial role in fungal developmental and morphogenetic processes, including *Rho*, *Cdc42*, and *Rac* [43]. Under different culture conditions of *T. asahii*, the expression of *CdC42* was found to significantly increased after the transition from the yeast phase to the hyphal phase, while the relative mRNA expression levels of *Ras1*, *Rac1*, and *Rho1* were all significantly higher in the hyphal phase than in the yeast phase [44, 45]. The coordinated regulation of these genes induced the transition of *T. asahii* from the hyphal phase to the yeast phase.

The overexpression of *TaADH_like* slightly enhances fluconazole resistance in *T. asahii*

In *C. albicans*, a fluconazole MIC ≤ 8 μg/mL indicates susceptibility to fluconazole [46], but no such criteria have been established for *T. asahii*. In this study, fluconazole resistance in *T. asahii* increased from 2 to 4 μg/mL to 8 μg/mL following overexpression of *TaADH_like*. Biofilm activity was significantly higher in TaADH_like^{OE} than WT. Arthroconidia of *T. asahii* promote biofilm formation by enhancing cell adhesion [21, 47, 48]. TaADH_like^{OE} was transitioned from the hyphae phase to the

yeast phase, and the increase in arthroconidia enhanced biofilm formation. Biofilm formation can hinder the entry of drugs into fungal cells [15]. In MIC experiment, the adhesion and growth of *T. asahii* on 96-well cell culture plates may contribute to the slight increase in fluconazole resistance observed in TaADH_like^{OE}. Although the overexpression of the *TaADH_like* only induces a slight increase in drug resistance, it does contribute to enhancing the drug resistance of *T. asahii.* Therefore, we speculate that *TaADH_like* is a potential gene associated with drug resistance in *T. asahii*.

The overexpression of *TaADH_like* maintains *T. asahii* growth under anaerobic conditions

In organisms, alcohol dehydrogenase (ADH) catalyzes the NAD^+-mediated interconversion between ethanol and acetaldehyde [49]. This catalytic process is also accompanied by the production of the energy molecule ATP, which plays a crucial role in the resistance of organisms to adverse stress [50]. Moreover, *ADH* is regulated by oxygen. In *Pichia pastoris*, the transcription of *ADH1* is regulated by oxygen, with higher expression under oxygen-limited conditions than under aerobic conditions. Its expression is inversely correlated with oxygen concentration, increasing as oxygen levels decrease [51]. Similarly, *Adh1* is up-regulated under hypoxic conditions in *Fusarium spinosum* and *Metarhizium* [52, 53]. In this study, we found that overexpression of *TaADH_like* increased the tolerance of strains under hypoxic conditions, consistent with the results of previous studies.

HOG-MAPK pathway May reduce pathogenicity by influencing its colonisation

In *S. cerevisiae*, the *HOG1* pathway is activated by two distinct upstream branches, *Sln1* and *Sho1* [54]. The *Sln1* branch consists of the transmembrane histidine kinase receptor *Sln1*, the phosphotransporter protein *Ypd1*, the response regulator *Ssk1*, and the MAPKKK *Ssk2/Ssk22*, and the *Sho1* branch consists of the transmembrane osmolality receptor *Sho1*, the small G protein *Cdc42*, the PAK kinase *Ste20*, and the MAPKKK *Ste11* [55]. *PBS2* is a scaffolding protein that can be activated by *Ssk2/Ssk22* and *Ste11* to further activate *HOG1* in response to hyperosmotic stress [56]. In *C. albicans*, Ssk2 and Ssk22 merge into a single gene, Ssk2, and *Ste11* is not involved in the regulation of the *Hog1* signaling pathway [57]. In *C. albicans*, *Hog1* is regulated only by *Ssk2* and is not affected by *Ste11* [58]. This is a marked difference from the *HOG1* signaling pathway in *S. cerevisiae*. In this study, *SSK2* was not annotated in *T. asahii*, and only *SSK22* was present. The *Sln1* pathway consists of *CnNIK1* (*Sln1*), *CnHHK2* (*Ypd1*), *SSK1*, and *SSK22*.The *Sho1* branch consists of *Sho1*, *Cdc42*, *Ste20*, and *Ste11*. However, *Ste11* was not differentially expressed under high osmotic conditions, and it is presumed that *Ste11* is also not involved in the regulation of the *HOG1* signaling pathway in *T. asahii*. Except for *Ste11*, *Sho1* of *HOG1* pathway was significantly down-regulated and *CnNIK1* gene appeared significantly up-regulated in *T. asahii*, presumably the *Sho1* pathway was suppressed by overexpression of *TaADH_like*, and *CnNIK1* acted as the main pathway in response to osmotic stress. There are no unannotated *PBS2*-associated genes in *T. asahii*, which may be similar to *C. albicans*, where *HOG1* is directly regulated by genes such as *SSK22*.

In *C. albicans*, the Hog MAPK pathway regulates the formation of hypha, which affects the virulence of the strain, and *Hog1* inhibits the yeast-to-hyphae transition through downstream components [59]. *Hog1* can act as a repressor of the yeast-to-hypha transition and an inducer of chlamydospore formation in *C. albicans* [60]. Additionally, *Hog1* has been found to be involved in the colonization of the mouse intestine by *C. albicans* [61]. The virulence of *hog1* defective mutant of *T. asahii* to silkworm was weakened [62]. In this study, *HOG1* was significantly down-regulated, and it is speculated that the Hog MAPK pathway was involved in the hyphae-to-yeast transition of *T. asahii* and reduced the colonisation ability of TaADH_like^{OE}.

The overexpression of *TaADH_like* reduces the pathogenicity of *T. asahii*

The ability to switch between yeast and hyphal is necessary for virulence [63, 64]. Both forms play crucial roles during infection. The yeast form may disseminate via the bloodstream, spreading the organism to various host ecological niches, while the hyphal form is invasive, enabling the organism to evade phagocytosis [65]. In dimorphic ascomyces *C. albicans*, the reduction of hyphal formation ability reduced the virulence of *C. albicans* in mice, *Caenorhabditis Elegans* and *Galleria mellonella* [8]. The transformation of *T. asahii* clinical isolates from the hyphal phase to the yeast phase reduced the lethality of infection in mice, with the organism predominantly in the pseudohyphal form within host tissues [66]. In this study, overexpression of *TaADH_like* led to a shift of *T. asahii* from the hyphal phase to the yeast phase, resulting in reduced lethality in mice. WT exhibited stronger colonization of organs compared to TaADH_like^{OE}. Pathological histology revealed that the WT-inoculated mice developed pathological damage earlier and exhibited more severe damage than the TaADH_like^{OE}-inoculated mice. In conclusion, overexpression of *TaADH_like* caused *T. asahii* to shift from the hypha phase to the yeast phase, thereby reducing its pathogenicity.

Alcohol dehydrogenase is widely present in organisms, but the genome-wide information of many fungi has not been precisely annotated. The genome-wide information

of *T. asahii* was annotated to the chromosome level for the first time in this laboratory. Although the article was explored by model strains *C. albicans* and *S. cerevisiae*, there is a lack of fungi from the same family and genus to jointly explore the evolutionary level of *T. asahii*. It is hoped that this will be addressed in future studies.

Conclusion

Alcohol dehydrogenase is involved in pathogenicity regulation of *T. asahii.* The *T. asahii* ADH gene family contains six members. Overexpression of *TaADH_like* reduced sensitivity to hypoxic environments, conversion of *T. asahii* from hyphae to yeast phase, slower growth, diminishes colonisation ability, reduced damage to organ tissues and lowers lethality. Increased osmotic stress sensitivity and the involvement of the HOG MAPK pathway in the hyphae-to-yeast transition reduce the colonization ability of *T. asahii.* Furthermore, the overexpression of *TaADH_like* promoted biofilm formation and led to a slight enhancement in fluconazole resistance in *T. asahii.*

Supplementary Information

The online version contains supplementary material available at https://doi.org/10.1186/s12864-025-11546-5.

Supplementary Material 1

Acknowledgements
Not applicable.

Author contributions
ZL (Zhen Liu), XM and XZ analyse the data and Write-Original draft preparation. ZL (Zhiguo Li) prepares the sample. RL (Rongyan Luo) and RL (Ruiguo Liu) check the data. WW and MS (Muhammad Salman Tahir) have been substantially revised. CW and YG conceived and designed the analysis. All authors read and approved the final manuscript.

Funding
This work was supported by the Sichuan Beef Cattle Innovation team of the National Modern Agricultural Industry Technology System (grant number SCCXTD_2023-13).

Data availability
The T. asahii datasets generated during the current study are available in the Genome Sequence Archive at the National Genomics Data Center, China National Center for Bioinformation/Beijing Institute of Genomics, Chinese Academy of Sciences repository, GSA: CRA014197. The S. cerevisiae datasets generated during the current study are available in the Saccharomyces Genome Database repository, GCA_000146045. The C. albicans datasets generated during the current study are available in the International Nucleotide Sequence Database Collaboration repository, GCA_000182965. The data of GCA_000146045 and GCA_000182965 are publicly available on Ensembl Fungi (http://fungi.ensembl.org/index.html). The genome assemblies are R64-1-1 and GCA000182965v3 respectively.

Declarations

Ethics approval and consent to participate
All animal experiments were approved by the Institutional Animal Care and Use Committee of Sichuan Agricultural University (permit number: DYY-S20231020).

Consent for publication
Not applicable.

Competing interests
The authors declare no competing interests.

Received: 7 October 2024 / Accepted: 28 March 2025
Published online: 07 April 2025

References

1. Li H, Guo M, Wang C, Li Y, Fernandez AM, Ferraro TN, Yang R, Chen Y. Epidemiological study of trichosporon Asahii infections over the past 23 years. Epidemiol Infect. 2020;148:e169.
2. Mulè A, Rossini F, Sollima A, Lenzi A, Fumarola B, Amadasi S, Chiari E, Lorenzotti S, Saccani B, Van Hauwermeiren E, et al. Trichosporon Asahii infective endocarditis of prosthetic valve: A case report and literature review. Antibiot (Basel Switzerland). 2023;12(7):1181.
3. Parrozzani R, Marchione G, Midena G. Endogenous trichosporon Asahii retinitis. Ophthalmology. 2022;129(1):66.
4. Schnur J, Hawco C, Fonarov I, Casadesus D. Rare cutaneous manifestation of trichosporon Asahii. BMJ Case Rep. 2021;14(6):e243659.
5. Vibha M, Charu N, Neelam G, Nidhi S, Sunvir R, Jagdish C. A comprehensive review of trichosporon spp.: an invasive and emerging fungus. Cureus. 2021;13(8):e17345.
6. Francisco EC, de Almeida Junior JN, Queiroz-Telles F, Aquino VR, Mendes AVA, de Oliveira Silva M, Castro P, Guimarães T, Ponzio V, Hahn RC, et al. Correlation of trichosporon Asahii genotypes with anatomical sites and antifungal susceptibility profiles: data analyses from 284 isolates collected in the last 22 years across 24 medical centers. Antimicrob Agents Chemother. 2021;65(3):e01104–01120.
7. Malacrida AM, Corrêa JL, Barros ILE, Veiga FF, Pereira E, Negri M, Svidzinski TIE. Hospital trichosporon Asahii isolates with simple architecture biofilms and high resistance to antifungals routinely used in clinical practice. J De Mycol Medicale. 2023;33(2):101356.
8. Song Y, Li S, Zhao Y, Zhang Y, Lv Y, Jiang Y, Wang Y, Li D, Zhang H. ADH1 promotes Candida albicans pathogenicity by stimulating oxidative phosphorylation. Int J Med Microbiology: IJMM. 2019;309(6):151330.
9. Breunig KD, Bolotin-Fukuhara M, Bianchi MM, Bourgarel D, Falcone C, Ferrero II, Frontali L, Goffrini P, Krijger JJ, Mazzoni C, et al. Regulation of primary carbon metabolism in Kluyveromyces lactis. Enzym Microb Technol. 2000;26(9–10):771–80.
10. DafaAlla T, Abdalla M, El-Arabey AA, Eltayb WA, Mohapatra RK. Botrytis cinerea alcohol dehydrogenase mediates fungal development, environmental adaptation and pathogenicity. J Biomol Struct Dyn. 2022;40(23):12426–38.
11. da Silva Dantas A, Lee KK, Raziunaite I, Schaefer K, Wagener J, Yadav B, Gow NAR. Cell biology of Candida albicans–host interactions. Curr Opin Microbiol. 2016;34:111–8.
12. Sudbery P, Gow N, Berman J. The distinct morphogenic States of Candida albicans. Trends Microbiol. 2004;12(7):317–24.
13. Montoya AM, Elizondo-Zertuche M, Treviño-Rangel RdJ, Becerril-García M, González GM. Biofilm formation and antifungal susceptibility of trichosporon Asahii isolates from Mexican patients. Revista Iberoamericana De Micología. 2018;35(1):22–6.
14. Duarte-Oliveira C, Rodrigues F, Gonçalves SM, Goldman GH, Carvalho A, Cunha C. The cell biology of the Trichosporon-Host interaction. Front Cell Infect Microbiol. 2017;7:118.
15. Pereira R, dos Santos Fontenelle RO, de Brito EHS, de Morais SM. Biofilm of Candida albicans: formation, regulation and resistance. J Appl Microbiol. 2021;131(1):11–22.
16. Ma X, Liu Z, Zeng X, Li Z, Luo R, Liu R, Wang C, Gu Y. Genome-Wide identification and characterization of the Medium-Chain dehydrogenase/reductase superfamily of trichosporon Asahii and its involvement in the regulation of fluconazole resistance. J fungi (Basel Switzerland). 2024;10(2):123.
17. Kumar S, Stecher G, Li M, Knyaz C, Tamura K. MEGA X: molecular evolutionary genetics analysis across computing platforms. Mol Biol Evol. 2018;35(6):1547–9.
18. He Z, Zhang H, Gao S, Lercher MJ, Chen W-H, Hu S. Evolview v2: an online visualization and management tool for customized and annotated phylogenetic trees. Nucleic Acids Res. 2016;44(W1):W236–41.

19. Bailey TL, Johnson J, Grant CE, Noble WS. The MEME suite. Nucleic Acids Res. 2015;43(W1):W39–49.
20. Chen C, Wu Y, Li J, Wang X, Zeng Z, Xu J, Liu Y, Feng J, Chen H, He Y, et al. TBtools-II: A one for all, all for one bioinformatics platform for biological big-data mining. Mol Plant. 2023;16(11):1733–42.
21. Ma X, Liu H, Liu Z, Wang Y, Zhong Z, Peng G, Gu Y. Trichosporon Asahii PLA2 gene enhances drug resistance to Azoles by improving drug efflux and biofilm formation. Int J Mol Sci. 2023;24(10):8855.
22. Matsumoto Y, Yamazaki H, Yamasaki Y, Tateyama Y, Yamada T, Sugita T. A novel silkworm infection model with fluorescence imaging using Transgenic trichosporon Asahii expressing eGFP. Sci Rep. 2020;10(1):10991.
23. Ma X, Liu Z, Yue C, Wang S, Li X, Wang C, Ling S, Wang Y, Liu S, Gu Y. High-throughput sequencing and characterization of potentially pathogenic fungi from the vaginal mycobiome of giant panda (Ailuropoda melanoleuca) in estrus and non-estrus. Front Microbiol. 2024;15:1265829.
24. (CLSI) TCaLSI. M27-A3 Reference method for broth dilution antifungal susceptibility testing of yeasts: approved standard-Third Edition. In.; 2008.
25. Ramage G, Vande Walle K, Wickes BL, López-Ribot JL. Standardized method for in vitro antifungal susceptibility testing of Candida albicans biofilms. Antimicrob Agents Chemother. 2001;45(9):2475–9.
26. Lee H, Bien CM, Hughes AL, Espenshade PJ, Kwon-Chung KJ, Chang YC. Cobalt chloride, a hypoxia-mimicking agent, targets sterol synthesis in the pathogenic fungus Cryptococcus neoformans. Mol Microbiol. 2007;65(4):1018–33.
27. Zhu S, Zhao X, Liu H. Recent advances in chemical derivatization-based chromatography-mass spectrometry methods for analysis of aldehyde biomarkers. Chin J Chromatogr. 2021;39(08):845–54.
28. Chung CY, Duchen MR. A plate Reader-Based measurement of the cellular ROS production using dihydroethidium and mitosox. Methods Mol Biology (Clifton NJ). 2022;2497:333–7.
29. McCarthy CGP, Fitzpatrick DA. Pan-genome analyses of model fungal species. 2019, 5(2).
30. Lopes JP, Lionakis MS. Pathogenesis and virulence of Candida albicans. Virulence. 2022;13(1):89–121.
31. Cañestro C, Albalat R, Hjelmqvist L, Godoy L, Jörnvall H, Gonzàlez-Duarte R. Ascidian and amphioxus adh genes correlate functional and molecular features of the ADH family expansion during vertebrate evolution. J Mol Evol. 2002;54(1):81–9.
32. Mo C, Xie C, Wang G, Liu J, Hao Q, Xiao X, Xiao Y. Genome-Wide identification and characterization of the Cyclophilin gene family in the nematophagous fungus purpureocillium lilacinum. Int J Mech Sci. 2019;20(12):2978.
33. Park HS, Ni M, Jeong KC, Kim YH, Yu JH. The role, interaction and regulation of the Velvet regulator VelB in Aspergillus Nidulans. PLoS ONE. 2012;7(9):e45935.
34. Karakkat BB, Gold SE, Covert SF. Two members of the ustilago Maydis Velvet family influence teliospore development and virulence on maize seedlings. Fungal Genet Biology: FG B. 2013;61:111–9.
35. Wu JQ, Bähler J, Pringle JR. Roles of a fimbrin and an alpha-actinin-like protein in fission yeast cell polarization and cytokinesis. Mol Biol Cell. 2001;12(4):1061–77.
36. Fischer R, Timberlake WE. Aspergillus Nidulans apsa (anucleate primary sterigmata) encodes a coiled-coil protein required for nuclear positioning and completion of asexual development. J Cell Biol. 1995;128(4):485–98.
37. Briza P, Eckerstorfer M, Breitenbach M. The sporulation-specific enzymes encoded by the DIT1 and DIT2 genes catalyze a two-step reaction leading to a soluble LL-dityrosine-containing precursor of the yeast spore wall. Proc Natl Acad Sci USA. 1994;91(10):4524–8.
38. Pihet M, Vandeputte P, Tronchin G, Renier G, Saulnier P, Georgeault S, Mallet R, Chabasse D, Symoens F, Bouchara JP. Melanin is an essential component for the integrity of the cell wall of Aspergillus fumigatus conidia. BMC Microbiol. 2009;9:177.
39. Mariscal J, Thomas DP, Cleary IA. Examining the effects of BRG1 over-expression on Candida albicans strains growing as pseudohyphae. Folia Microbiol. 2023;68(4):571–7.
40. Mao Y, Solis Norma V, Filler Scott G, Mitchell Aaron P. Functional dichotomy for a hyphal repressor in Candida albicans. mBio. 2023;14(2):e00134–00123.
41. Murad AM, Leng P, Straffon M, Wishart J, Macaskill S, MacCallum D, Schnell N, Talibi D, Marechal D, Tekaia F, et al. NRG1 represses yeast-hypha morphogenesis and hypha-specific gene expression in Candida albicans. EMBO J. 2001;20(17):4742–52.
42. Cleary Ian A, Mulabagal P, Reinhard Sara M, Yadev Nishant P, Murdoch C, Thornhill Martin H, Lazzell Anna L, Monteagudo C. Thomas Derek P, Saville Stephen P: pseudohyphal regulation by the transcription factor Rfg1p in Candida albicans. Eukaryot Cell. 2010;9(9):1363–73.
43. Si H, Rittenour WR, Harris SD. Roles of Aspergillus Nidulans Cdc42/Rho GTPase regulators in hyphal morphogenesis and development. Mycologia. 2016;108(3):543–55.
44. Chen S, Zhou J, Lv u, Liao Y, Li H, Wang R, Yang R. The differences of Cdc42 expression between the yeast and hyphal forms of trichosporon Asahiis. Chin J Dermatovenereology. 2016;30(06):569–73.
45. Chen S, Zhou J, Liao Y, Li H, Wang R, Gen B, Lv u, Yang R. Differential expression of Ras1, Rac1, and Rho1 genes in the yeast and hyphal forms of trichosporon Asahiis. Chin J Dermatovenereology. 2017;50(03):207–10.
46. Rex JH, Pfaller MA, Galgiani JN, Bartlett MS, Espinel-Ingroff A, Ghannoum MA, Lancaster M, Odds FC, Rinaldi MG, Walsh TJ, et al. Development of interpretive breakpoints for antifungal susceptibility testing: conceptual framework and analysis of in vitro-in vivo correlation data for fluconazole, Itraconazole, and Candida infections. Subcommittee on antifungal susceptibility testing of the National committee for clinical laboratory standards. Clin Infect Diseases: Official Publication Infect Dis Soc Am. 1997;24(2):235–47.
47. Kurakado S, Miyashita T, Chiba R, Sato C, Matsumoto Y, Sugita T. Role of arthroconidia in biofilm formation by trichosporon Asahii. Mycoses. 2021;64(1):42–7.
48. Kim YG, Lee JH, Park JG, Lee J. Inhibition of Candida albicans and Staphylococcus aureus biofilms by centipede oil and Linoleic acid. Biofouling. 2020;36(2):126–37.
49. Hageman RH, Flesher D. The effect of an anaerobic environment on the activity of alcohol dehydrogenase and other enzymes of corn seedlings. Arch Biochem Biophys. 1960;87(2):203–9.
50. Zhang R, Xuan L, Ni L, Yang Y, Zhang Y, Wang Z, Yin Y, Hua J. ADH gene cloning and identification of Flooding-Responsive genes in Taxodium distichum (L.) rich. Plants (Basel). 2023;12(3):678.
51. Cho JY, Jeffries TW. Transcriptional control of ADH genes in the xylose-fermenting yeast Pichia stipitis. Appl Environ Microbiol. 1999;65(6):2363–8.
52. Corrales Escobosa AR, Rangel Porras RA, Meza Carmen V, Gonzalez Hernandez GA, Torres Guzman JC, Wrobel K, Wrobel K, Roncero MI, Gutierrez Corona JF. Fusarium oxysporum Adh1 has dual fermentative and oxidative functions and is involved in fungal virulence in tomato plants. Fungal Genet Biology: FG B. 2011;48(9):886–95.
53. Zhang E, Cao Y, Xia Y. Ethanol dehydrogenase I contributes to growth and sporulation under low oxygen condition via detoxification of acetaldehyde in metarhizium acridum. Front Microbiol. 2018;9:1932.
54. O'Rourke SM, Herskowitz I, O'Shea EK. Yeast go the whole HOG for the hyperosmotic response. Trends Genet. 2002;18(8):405–12.
55. Tatebayashi K, Yamamoto K, Tomida T, Nishimura A, Takayama T, Oyama M, Kozuka-Hata H, Adachi-Akahane S, Tokunaga Y, Saito H. Osmostress enhances activating phosphorylation of Hog1 MAP kinase by mono-phosphorylated Pbs2 MAP2K. EMBO J. 2020;39(5):e103444.
56. Tatebayashi K, Yamamoto K, Tomida T, Nishimura A, Takayama T, Oyama M, Kozuka-Hata H, Adachi-Akahane S, Tokunaga Y, Saito H. Osmostress enhances activating phosphorylation of Hog1 MAP kinase by mono-phosphorylated Pbs2 MAP2K. EMBO J. 2020;39(5):e103444.
57. Liu J, Wang ZK, Sun HH, Ying SH, Feng MG. Characterization of the Hog1 MAPK pathway in the entomopathogenic fungus Beauveria Bassiana. Environ Microbiol. 2017;19(5):1808–21.
58. Cheetham J, Smith DA, da Silva Dantas A, Doris KS, Patterson MJ, Bruce CR, Quinn J. A single MAPKKK regulates the Hog1 MAPK pathway in the pathogenic fungus Candida albicans. Mol Biol Cell. 2007;18(11):4603–14.
59. Chen H, Zhou X, Ren B, Cheng L. The regulation of hyphae growth in Candida albicans. Virulence. 2020;11(1):337–48.
60. Eisman B, Alonso-Monge R, Román E, Arana D, Nombela C, Pla J. The Cek1 and Hog1 Mitogen-Activated protein kinases play complementary roles in cell wall biogenesis and chlamydospore formation in the fungal pathogen Candida albicans. Eukaryot Cell. 2006;5(2):347–58.
61. Prieto D, Román E, Correia I, Pla J. The HOG pathway is critical for the colonization of the mouse Gastrointestinal tract by Candida albicans. PLoS ONE. 2014;9(1):e87128.
62. Matsumoto Y, Sugiyama Y, Nagamachi T, Yoshikawa A, Sugita T. Hog1-mediated stress tolerance in the pathogenic fungus trichosporon Asahii. Sci Rep. 2023;13(1):13539.
63. Mayer FL, Wilson D, Hube B. Candida albicans pathogenicity mechanisms. Virulence. 2013;4(2):119–28.
64. Gow NAR, Brown AJP, Odds FC. Fungal morphogenesis and host invasion. Curr Opin Microbiol. 2002;5(4):366–71.

65. Jacobsen ID, Wilson D, Wächtler B, Brunke S, Naglik JR, Hube B. Candida albicans dimorphism as a therapeutic target. Expert Rev anti-infective Therapy. 2012;10(1):85–93.
66. Peng Y, Tian Y, Liao Y. The comparative analysis of the fatality rate of the mice infected by resistant or senstive T.asahii strains. J Practical Dermatology. 2019;12(5):263–6.

Publisher's note